phys. stat. sol. (a) **205**, No. 11, 2673–2678 (2008) / **DOI** 10.1002/pssa.200824233

physica status solidi a
www.pss-a.com
applications and materials science

Focused-ion-beam fabrication of ZnO nanorod-based UV photodetector using the in-situ lift-out technique

Oleg Lupan[*,1,2], Lee Chow[,1], Guangyu Chai[3], Leonid Chernyak[1], Olena Lopatiuk-Tirpak[1], and Helge Heinrich[1,4]**

[1] Department of Physics, University of Central Florida, P.O. Box 162385, Orlando, USA
[2] Department of Microelectronics and Semiconductor Devices, Technical University of Moldova, Stefan cel Mare Blvd. 168, 2004, Chisinau, Moldova
[3] Apollo Technologies, Inc., 205 Waymont Court, S111, FL 32746, Lake Mary, USA
[4] Advanced Materials Processing and Analysis Center, and Department of Mechanical, Materials, and Aerospace Engineering, University of Central Florida, P.O. Box 162385, Orlando, USA

Received by M. Shur 26 February 2008, revised 11 June 2008, accepted 12 June 2008
Published online 15 August 2008

PACS 42.79.Pw, 81.05.Dz, 81.10.Dn, 85.40.Hp, 85.60.Gz

[*] Corresponding author: e-mail lupan@physics.ucf.edu; lupanoleg@yahoo.com, Phone: +1 407 823 52117, Fax: +1 407 823 5112
[**] e-mail chow@mail.ucf.edu, Phone: +1 407 823 2333, Fax: +1 407 823 5112

ZnO nanorods and nanowires are promising candidates as new types of high-sensitivity ultraviolet (UV) photodetectors due to their wide bandgap and large aspect ratio. In this study, single-crystalline ZnO nanorods were grown on glass substrates by a hydrothermal method. Specific structural, morphological, electrical, and optical measurements were carried out. A single ZnO nanorod-based photodetector was fabricated using the in-situ lift-out technique in a focused ion beam (FIB/SEM) instrument and characterized. With a source wavelength of 370 nm and an applied bias of 1 V, the responsivity of the ZnO nanorod is 30 mA/W. The single ZnO nanorod photodetector exhibits an ultraviolet (UV) photoresponse promising for potential applications as cost-effective UV detectors.

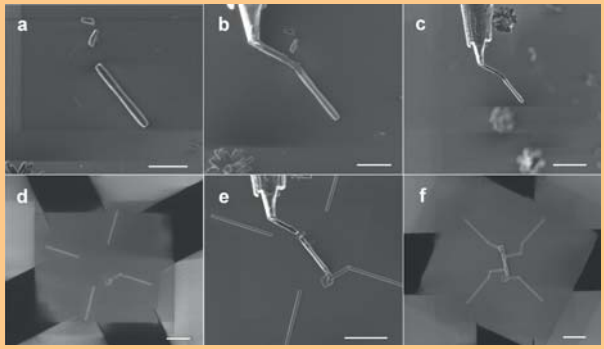

Secondary electron images in the focused ion-beam system showing the steps of the in-situ lift-out fabrication procedure in the FIB/SEM instrument.

1 Introduction Recently, much research has been focused on developing compact high-performance solid-state photodetectors in the ultraviolet (UV) spectral range [1–4]. High-tech applications of short-wavelength UV detectors range from commercial to military uses, and from biological and chemical sensing to flame detection and space communications, etc. [3, 5]. One major factor, which stimulates the development of new UV photodetectors is the growing "ozone hole" near the Antarctic linked to a growing number of cancer and skin illnesses [6].

UV detection using photomultiplier tubes [7] requires bulky, fragile and heavy equipment. Solid-state UV photodetectors are more efficient and lightweight [1, 8] and can be easily incorporated in different novel types of micro/nanosystems, such as in devices integrated in cell phones. These portable devices can help people to monitor their exposure to solar UV radiation.

With the development of optoelectronic nanodevices fabricated on wide-bandgap nanomaterials, high-performance UV photodetectors with high responsivity, line-

arity with optical power, low noise and high spectral selectivity can be produced. Analogous to III–V materials, ZnO possesses high UV photosensitivity that is most important for UV photodetection.

Zinc oxide is one of the most widely used oxide materials owing to its versatile characteristics like radiation hardness [9], high chemical stability, high optical gain (300 cm^{-1}) [10, 11], high-temperature resistance, and flexibility in fabrication [12, 13] that are extremely important for practical optoelectronic devices. However, fabrication of ultraviolet photodetectors using zinc oxide is still difficult due to the high cost of synthesis for high-quality ZnO single crystals.

ZnO nanorods/nanowires as optoelectronic materials are promising for next-generation UV photodetection applications due to their wide and direct bandgap ($E_g \sim 3.3$ eV at room temperature) and large surface-to-volume ratio. The large exciton binding energy of 60 meV makes ZnO a potential candidate for low-threshold blue/UV lasers that can be integrated with photodetectors [14, 15]. Nanosensors fabricated from ZnO with a larger surface-to-volume ratio have better characteristics [12, 16–18] and have the additional advantage of being insensitive to visible light [1].

In this letter, we report the growth of ZnO nanorods by a hydrothermal method and the focused-ion-beam fabrication of single ZnO nanorod-based UV photodetectors. The physical properties of the as-grown ZnO nanorods and the optical properties of fabricated photodetectors are discussed.

2 Experimental The ZnO nanorods in this study were synthesized via the hydrothermal method, which has been reported in our previous work [19]. This technique was found to be quite advantageous from the viewpoint of environmental impact, easy scalability, time saving and low production cost in comparison with other techniques.

In the synthesis process, all the reagents were analytically pure and used without further purification. Zinc sulfate $Zn(SO_4)\cdot 7H_2O$ and ammonia solution NH_4OH (29.6%) were dissolved in 50 ml of DI water until complete dissolution was achieved at room temperature. The solution was stirred vigorously to obtain a transparent solution. Then, the glass substrates were placed inside the aqueous solution in a hydrothermal reactor. The setup temperature was quickly increased to 90–95 °C and kept constant for 10 min without any stirring. Variation of the synthesis conditions such as overall concentration of precursors and temperature allow a certain degree of control on the growth rate and morphology of the obtained nanorods/nanowires.

The resulting ZnO nanorods were then annealed for 20 s at 650 °C in air. The crystalline quality and orientations of as-prepared ZnO nanorods were analyzed by X-ray diffraction (XRD). The stoichiometry was measured by energy-dispersive X-ray analysis (EDX) and the morphology of the products was analyzed by scanning electron microscopy (SEM). The morphology is considered to play a vital role in nanodevice applications. Transmission electron microscopy (TEM) confirmed that the nanorods are crystalline. High spatial resolution cathodoluminescence spectroscopy measurements were carried out at room temperature using a Gatan MonoCL3 cathodoluminescence system, which is integrated with a Philips XL 30 SEM. The emitted radiation was analyzed using a single grating (1200 lines/mm, blazed at 500 nm) and a Hamamatsu photomultiplier tube with sensitivity in the 185–850 nm range. An electron-beam accelerating voltage of 10 kV was used, corresponding to an electron penetration depth of about 0.5 μm. The focused ion beam (FIB) in-situ lift-out technique was employed for the photodetector fabrication. Current–voltage (I–V) characteristics were measured using a semiconductor parameter analyzer with input impedance of 2.00×10^8 Ω. The UV sensitivity was measured using a two-terminal ZnO nanorod device. The readings were taken after a UV light was turned on. The UV source is a Hg lamp with an incident peak wavelength of 370 nm.

3 Results and discussions

3.1 Structural characterization Indexed XRD scans on the ZnO nanorods in the range of 25–90° show a dominant sharp peak at 34.4°, which confirms the c-axis oriented (002) plane growth (Fig. 1). It can be seen that all diffraction peaks are from crystalline ZnO with the hexagonal wurtzite structure. The scattering data are in agreement with the Joint Committee on Powder Diffraction Standards (JCPDS) card for ZnO (JCPDS 036-1451) [20].

In Fig. 1, the detected (hkl) peaks are at 2θ values of 31.7°, 34.4°, 36.2°, 47.5°, 56.6°, and 62.8°, corresponding to the following lattice planes: (100), (002), (101), (102), (110), (103), respectively. The lattice constants a and c

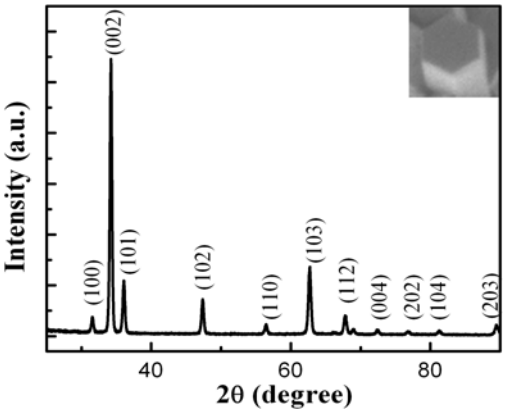

Figure 1 Indexed XRD scan for ZnO nanorods on a glass substrate synthesized by the hydrothermal method showing the preferential orientation of crystallites. The inset is an SEM image of a single ZnO nanorod showing a perfect hexagonal cross section.

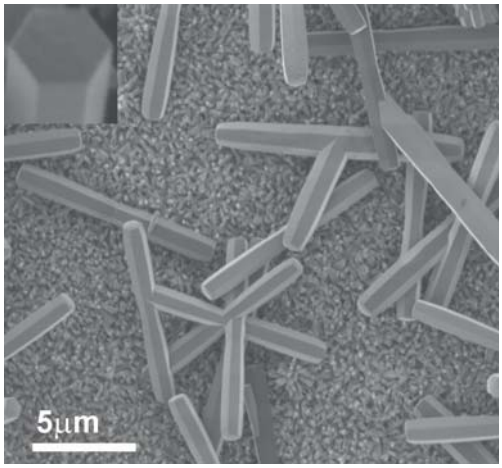

Figure 2 SEM images of the ZnO nanorods grown by the hydrothermal method from zinc sulfate and ammonia aqueous bath on glass substrates at 90–95 °C. The insert reveals the hexagonal symmetry of a rod.

were determined as $a = 0.3249$ nm, $c = 0.5206$ nm by using the following equation [21]

$$\frac{1}{d^2_{(hkl)}} = \frac{4}{3}\left(\frac{h^2 + hk + k^2}{a^2}\right) + \frac{l^2}{c^2}.$$

3.2 Morphological characterization The general morphologies of the as-synthesized ZnO nanorods were studied by scanning electron microscopy (SEM). A typical SEM image of the ZnO nanorods is shown in Fig. 2. The ZnO nanorods have an average radius of 300 nm and show perfectly flat surfaces with hexagonal symmetry. The lengths of ZnO nanorods are about 10 μm. According to our experimental results, the nanoarchitectures obtained by our process can be easily transferred to other substrates and can be handled by a focused-ion-beam (FIB) instrument.

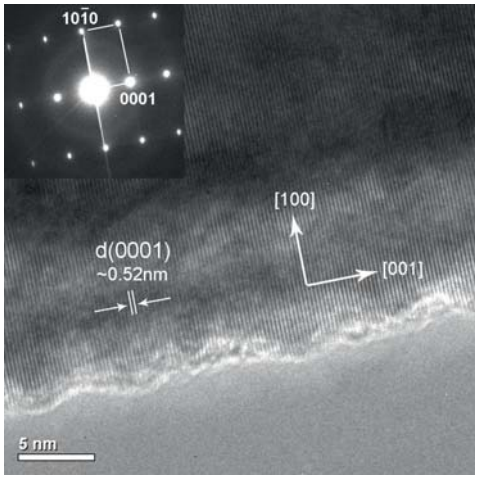

Figure 3 TEM image at a side edge of an as-synthesized ZnO nanorod and a typical SAED pattern of a single nanorod (see insert).

The detailed structural characterization of a single ZnO nanorod was performed by high-resolution transmission electron microscopy (HRTEM) with a FEI Tecnai F-30 microscope operating at 300 kV. A TEM image and a selective-area electron diffraction (SAED) pattern of an individual ZnO nanorod are shown in Fig. 3. The lattice fringes in all examined regions reveal no dislocations or stacking faults, illustrating that the nanorod is a defect-free single crystal.

The nanorods are straight and their surfaces are very smooth. A typical SAED pattern (inset in Fig. 3) taken from a ZnO nanorod can be indexed as a hexagonal structure of zinc oxide recorded along the [1$\bar{2}$10] zone axis, which indicates that the as-synthesized ZnO nanorods are single crystals.

From the TEM analysis, as in Fig. 3, it is clear that the ZnO nanorods are single crystalline and grow along the [0001] axis. The HRTEM image displays clearly resolved lattice distances of 0.52 nm along the long axis of a nanorod coinciding with the (0001) lattice spacing. These results confirm the XRD analysis that the ZnO nanorods are preferentially oriented in the [001] direction.

3.3 Nanofabrication of a photodetector by the in-situ lift-out technique Here, the in-situ lift-out procedure for the photodetector fabrication is described. A Keindiek Micromanipulator was mounted beside the stage in the FIB/SEM instrument. For the nanosensor preparation, a glass substrate was used and Al electrodes were deposited as templates with external electrodes/connections. The needle used for the lift-out step was an electropolished tungsten wire. The ZnO nanorods are transferred from the initial glass substrate to the Si/SiO_2 substrate in order to avoid charging problems during the fabrication process.

The next step in our procedure is to scan the surface of the intermediate Si/SiO_2 substrate for a conveniently oriented ZnO nanorod (Fig. 4a). Once found, the needle is lowered and brought into the FIB focus and its tip positioned at the close end of the intermediate nanorod as shown in Fig. 4b. In the in-situ lift-out process [19, 22–24], the attachment of a single intermediate nanorod (see Fig. 4b) on the top of the FIB needle [22, 23] permits an easy pick-up of the selected nanorod to be further processed. This step makes it possible to fabricate nanodevices much faster.

Once the desired nanorod is identified it is recommended to push the nanorod with the micromanipulator tip in order to make sure that it is not firmly attached to the substrate and is transferable. The *W* needle with the intermediate ZnO nanorod attached is then moved until it touches the desired ZnO nanorod. Then, the selected ZnO nanorod is attached to the end of the intermediate ZnO nanorod on the FIB needle as shown in Fig. 4b with Pt deposition to the joint. After the nanowelding of the selected ZnO nanorod with the micromanipulator the *W* needle and specimen is raised away from the substrate (Fig. 4c).

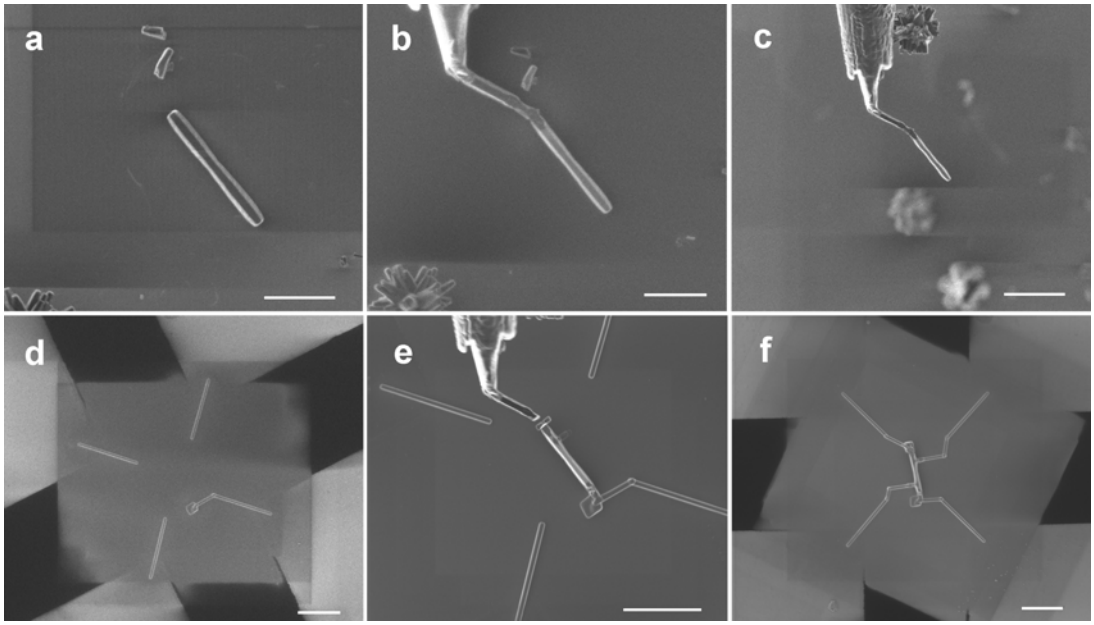

Figure 4 Secondary electron micrographs showing the steps of the in-situ lift-out fabrication procedure in the FIB/SEM system. (a) An intermediate ZnO nanorod on a Si/SiO_2 substrate; (b) needle with intermediate ZnO nanorod placed close to a single ZnO nanorod selected for UV photodetector fabrication; (c) a ZnO nanorod picked up by the needle, next to the FIB needle; (d) nanosensor substrate template (glass with Al contacts as contact electrodes); e) placement of the ZnO nanorod on substrate; (f) single nanorod welded to four electrode/external connections as final nanophotodetector. The scale bar is 5 μm.

Figure 4d shows the nanophotodetector substrate template (glass with Al contacts as contact electrodes). Using the micromanipulator, we carefully position the nanorod between the electrodes (Fig. 4e). In the last step, the nanorod is fixed to one of the predeposited electrodes/external contacts. The nanorod is cut (Fig. 4e) and the needle moves away from the substrate. Figure 4f shows a novel single ZnO nanorod-based photodetector fabricated by this in-situ lift-out technique in the FIB/SEM system. By this technique differently shaped photodetectors have been prepared.

3.4 Optical and UV sensing properties The room-temperature cathodoluminescence (CL) spectra of the ZnO nanorods are shown in Fig. 5. The CL emission spectrum of a single ZnO nanorod (Fig. 5) reveals a strong UV emission at 389 nm, which corresponds to the near-band-edge emission of ZnO. This strong ultraviolet emission coupled with a weak broad green emission band, suggests that the nanorod structures posses high crystal quality with minimum oxygen vacancies. High-quality ZnO nanorods are very important for UV sensors. Our results demonstrate that this hydrothermal method is capable of the growth of high-quality nanostructures with few defects for future optoelectronic nanodevices applications.

Here, we measured the current–voltage (I–V) curves of the ZnO nanorod fabricated acoording to the procedure outlined in Fig. 4. Figure 6 illustrates the characteristics of a four-terminal ZnO nanorod photodetector in ambient air. The four-probe I–V electrical measurements were performed by changing the bias voltages from +5 mV to −5 mV and vice versa. The voltage increment and delay time were set to 0.50 mV and 3 s.

Current–voltage measurements of the samples show linear characteristics in this range. The electrical resistivity of the ZnO nanorod was estimated to be about 0.20 Ω cm from the four-probe dc measurements. The I–V curves are linear, and the contact resistance was calculated to be about 200 Ω per contact, which is small compared to the

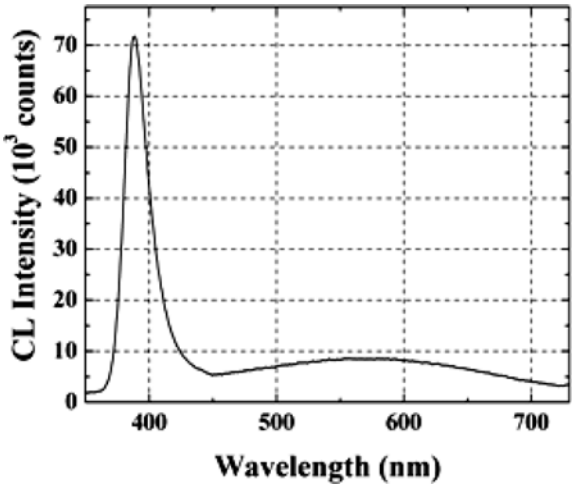

Figure 5 Cathodoluminescence (CL) spectrum of a one-dimensional ZnO nanorod.

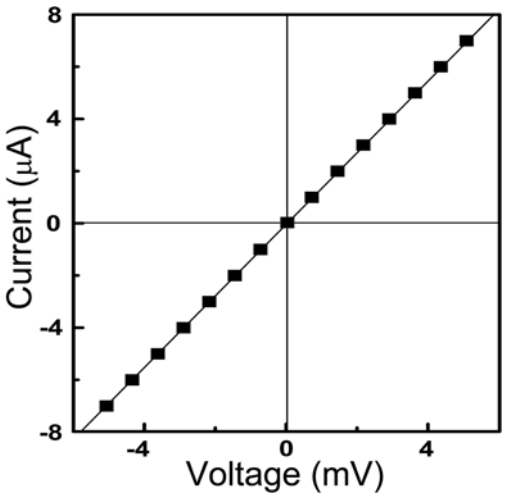

Figure 6 *I–V* characteristics of a single ZnO nanorod photodetector.

nanorod resistance of approximately 1 kΩ (between their middle contacts).

The room-temperature sensitivity of the single nanorod ZnO nanophotodetector to UV light is shown in Fig. 7. When the ZnO nanorod photodetector is illuminated by 370 nm UV light, the conductance increases with a time constant of a few minutes, as shown in Fig. 7. When the UV light is turned off, the conductance decreases back to within 10% of the initial value. The UV response is relatively fast for a ZnO-nanorod photodetector.

The UV response time is found to be around a few minutes and can be explained by the adsorption and photodesorption of ambient gas molecules such as O_2 or H_2O [25, 26]. As-grown ZnO nanorods adsorb oxygen molecules on the surface. This will take free electrons from the n-type ZnO nanorod to form a depletion region. After UV illumination of the photodetector the electron–hole (e^-–h^+) pairs will be generated. The holes (h^+) will migrate to the surface to discharge the chemisorbed oxygen ions and lowering the depletion layer near the surface

$$h^+ + O^-_{2ad} \rightarrow O_2(g)\,.$$

Due to the fact that the photon energy is higher than the bandgap of ZnO, UV radiation is absorbed by the ZnO nanorod, creating electron–hole pairs, which are further separated by the electric field inside the ZnO nanorod contributing to the increase of the conductivity.

After the exposure to UV radiation, the sensor is maintained for a recovery period. The sensor shows a relatively fast response and baseline recovery for UV detection. This suggests a reasonable recovery time. The quantity of photogenerated e^-–h^+ pairs depends on the intensity of UV exposure, and the discharge effect of the photogenerated holes on the chemisorbed oxygen. The holes will recombine with oxygen ions chemisorbed on the surface and eliminate the depletion region [25]. At the same time the electrons produced will contribute to conductivity. The oxygen adsorption at the surface of ZnO may also affect the response time [27–29].

Several photodetectors have been fabricated by the in-situ lift-out technique and have been investigated under identical conditions. Similar UV responses were observed.

The spectral response demonstrates that such a photodetector is indeed suitable for detecting UV radiation in the range of 300–400 nm.

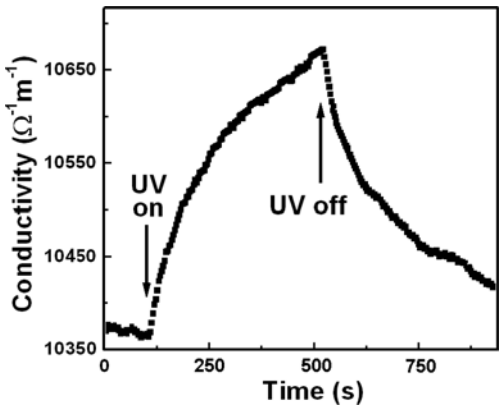

Figure 7 Conductivity response of the ZnO-nanorod-based UV photosensor fabricated by the in-situ lift-out technique in the FIB system.

4 Conclusions In summary, fabrication of a single ZnO-nanorod UV photodetector is demonstrated for the first time. An in-situ lift-out technique has been presented in detail to fabricate the single ZnO-nanorod-based photodetector. The photoresponse measurements indicate that the nanorod-based photodetector has reasonable recovery time and responsivity.

The prototype device shows a simple method for nanowire synthesis and demonstrates the possibility of constructing nanoscale photodetectors for nano-optics applications.

Acknowledgements Dr. L. Chow acknowledges partial financial support from Apollo Technologies, Inc. and the Florida High Tech Corridor Program. The research described in this publication was made possible in part by Award No. MTFP-1014B Follow-On of the Moldovan Research and Development Association (MRDA) and the U.S. Civilian Research and Development Foundation (CRDF).

References

[1] F. Masuoka, K. Ooba, H. Sasaki, H. Endo, S. Chiba, K. Maeda, H. Yoneyama, I. Niikura, and Y. Kashiwaba, phys. stat. sol. (c) **3**, 1238 (2006).

[2] S. J. Young, L. W. Ji, S. J. Chang, S. H. Liang, K. T. Lam, T. H. Fang, K. J. Chen, X. L. Du, and Q. K. Xue, Sens. Actuators A, Phys. **135**, 529 (2007).

[3] S. J. Young, L. W. Ji, T. H. Fang, S. J. Chang, Y. K. Su, and X. L. Du, Acta Mater. **55**, 329 (2007).
[4] Y. A. Goldberg, Semicond. Sci. Technol. **14**, R41 (1999).
[5] E. Monroy, F. Calle, J. L. Pau, E. Muñoz, F. Omnès, B. Beaumont, and P. Gibart, J. Cryst. Growth **230**, 537 (2001).
[6] T. V. Blank, Yu. A. Goldberg, and O. V. Konstantinov, Nucl. Instrum. Methods Phys. Res. A **487**, 60 (2002).
[7] J. L. Wiza, Nucl. Instrum. Methods **162**, 587 (1979).
[8] J. Cheng, Y. Zhang, and R. Guo, J. Cryst. Growth **310**, 57 (2008).
[9] F. D. Auret, S. A. Goodman, M. Hayes, M. J. Legodi, H. A. van Laarhoven, and D. C. Look, Appl. Phys. Lett. **79**, 3074 (2001).
[10] Y. Chen, D. M. Bagnall, H. Koh, K. Park, K. Hiraga, Z. Zhang, and T. Yao, J. Appl. Phys. **84**, 3912 (1998).
[11] A. Ohtomo, M. Kawasaki, Y. Sakurai, I. Ohkubo, R. Shiroki, Y. Yoshida, T. Yasuda, Y. Segawa, and H. Koinuma, Mater. Sci. Eng. B **56**, 263 (1998).
[12] S. S. Hullavarad, N. V. Hullavarad, P. C. Karulkar, A. Luykx, and P. Valdivia, Nanoscale Res. Lett. **2**, 161 (2007).
[13] T. Ma, M. Guo, M, Zhang, Y. Zhang, and X. Wang, Nanotechnology **18**, 035605 (2007).
[14] K. W. Liu, J. G. Ma, J. Y. Zhang, Y. M. Lu, D. Y. Jiang, B. H. Li, D. X. Zhao, Z. Z. Zhang, B. Yao, and D. Z. Shen, Solid State Electron. **51**, 757 (2007).
[15] A. Ohtomo, M. Kawasaki, Y. Sakurai, Y. Yoshida, H. Koinuma, P. Yu, Z. K. Tang, G. K. L. Wong, and Y. Segawa, Mater. Sci. Eng. B **54**, 24 (1998).
[16] X. L. Cheng, H. Zhao, L. H. Huo, S. Gao, and J. G. Zhao, Sens. Actuators B, Chem. **102**, 248 (2004).
[17] Ü. Özgür, Ya. I. Alivov, C. Liu, A. Teke, M. A. Reshchikov, S. Dogan, V. Avrutin, S.-J. Cho, and H. Morkoç, J. Appl. Phys. **98**, 041301 (2005).
[18] H. K. Yadav, K. Sreenivas, and V. Gupta, Appl. Phys. Lett. **90**, 172113 (2007).
[19] O. Lupan, L. Chow, G. Chai, B. R. Soldan, A. Naitabdi, A. Schulte, and H. Heinrich, Mater. Sci. Eng. B **145**, 57 (2007).
[20] Joint Committee on Powder Diffraction Standards, Powder Diffraction File No. 36-1451.
[21] B. D. Cullity and S. R. Stock, Elements of X-Ray Diffraction, (Prentice Hall, New Jersey, 2001), p. 619.
[22] O. Lupan, G. Chai, and L. Chow, Microelectron. J. **38**, 1211 (2007).
[23] a) O. Lupan, G. Chai, and L. Chow, Microelectron. Eng. (2008), DOI: 10.1016/j.mee.2008.06.021.
b) O. Lupan, G. Chai, and L. Chow, NSTI Nanotechnology Conference, Boston, Massachusetts, USA, 1–5 June 2008, Vol. 3, pp. 5–8.
[24] G. Chai, L. Chow, Dan Zhou, and S. R. Byahut, Carbon **43**, 2083 (2005).
[25] J. Suehiro, N. Nakagawa, S. Hidaka, M. Ueda, K. Imasaka, M. Higashihata, T. Okada, and M. Hara, Nanotechnology **17**, 2567 (2006).
[26] J. B. K. Law and J. T. L. Thong, Appl. Phys. Lett. **88**, 133114 (2006).
[27] P. Peumans, A. Yakimov, and S. R. Forrest, J. Appl. Phys. **93**, 3693 (2003).
[28] D. H. Zhang, J. Phys. D. **28**, 1273 (1995).
[29] Y. Liu, C. R. Gorla, S. Liang, N. Emanetoglu, Y. Lu, H. Shen, and M. Wraback, J. Electron. Mater. **29**, 69 (2000).

